The eye's aplanatic answer

PABLO ARTAL* AND JUAN TABERNERO

are in the Laboratorio de Óptica, Departamento de Física, Universidad de Murcia, Campus de Espinardo, (Edificio CiOyN), 30071 Murcia, Spain.
***e-mail: pablo@um.es**

The human eye is a simple, but extremely robust, optical instrument. Analysis by sophisticated wavefront-sensing technology and customized ray-tracing has now revealed that the eye is actually an aplanatic design, with the cornea and lens compensating each other's aberrations.

The optics of the human eye impose the first physical limit to vision when projecting the images of the world onto the retina. However, the human eye is a relatively simple optical device with only two elements: the cornea and the crystalline lens. Until recently, we did not have a complete understanding of its optical properties and imaging performance. The development of an accurate description of the eye's optics is not only vital because it provides an understanding of the most important optical system for humans; it also supports the optimization of the design of contact lenses, refractive surgery procedures and artificial intraocular lenses, for example. High-resolution retinal imaging based on adaptive optics[1,2] can also greatly benefit from a better description of the optics of the eye.

In the past decade, the application of new wavefront-sensing technology[3] has been instrumental in studying the eye. One of the most significant advancements has been the recognition that in the normal young eye, the optical properties of the eye's cornea and lens are tuned so that they compensate each other and thus produce an improved overall image quality with minimal optical aberration. In particular, it has been found that spherical aberration and comatic aberration (distorted imaging of off-axis objects, often known as coma) in the cornea tend to be balanced (compensated) by the crystalline lens[4–7]. Normal ageing disrupts this balance[8], mainly because of a change in lens spherical aberration from negative to positive values[9], whereas corneal spherical aberration remains approximately stable with age[10]. This knowledge of the eye's spherical aberration and coma has

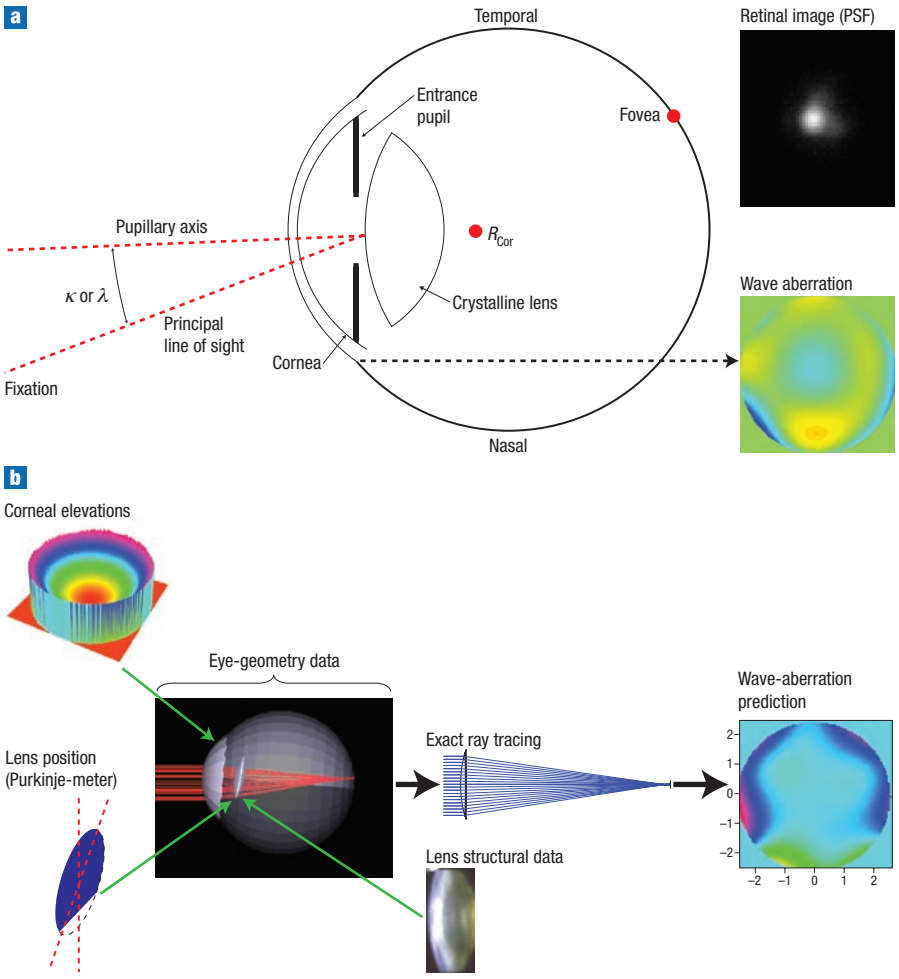

Figure 1 Modelling the eye. **a**, Schematic diagram of the human eye. The angle κ (also called λ) is shown as the angular distance between the fixation axis (principal line of sight) and the pupillary axis. An example of the wave-aberration function over the pupil is shown. When this wavefront is propagated, the ocular media forms an image over the fovea (the point of maximum resolution over the retina), called the point-spread function (PSF). R_{cor} is the centre of curvature of the cornea. **b**, Modelling the optical properties of the eye is possible after collecting all the experimental optical data: corneal surface topography, axial measurements, alignment and some structural data for the lens. It is then possible to predict the aberrations for each personalized model by ray tracing.

had important practical implications, including the design of various new types of intraocular lens (IOL) with aberration correction[11,12].

Recently, customized optical modelling[13,14] (where the aberrations of each eye can be predicted and then compared with actual data) has made great progress in explaining the optical mechanisms responsible for the compensation of aberrations within the eye[15]. By fine-tuning the predicted and the experimental results, it has become clear that the eye resembles an aplanatic optical design. This is a popular design in many man-made imaging systems, where good image quality is achieved by controlling and minimizing an optical system's spherical aberration and coma (often by using a series of complementary, specially shaped lenses). However, it is remarkable to think that what is considered the foundation of optical instrument design[16] is naturally occurring within the living human eye.

MEASURING THE EYE'S OPTICS

The imaging properties of the eye, in particular its aberrations, are produced by the shape of ocular surfaces, their location, relative alignment and the distribution of refractive indices. The two most commonly used functions to describe the eye's optical performance are the wave aberration and the point-spread function. The point-spread function represents the image formed on the retina in response to a point source of light. The wave aberration is defined as the difference between the perfect (spherical) and real wavefronts for every point over the eye's pupil. It is typically represented as a two-dimensional map, where each colour level represents the amount of wave aberration, expressed in micrometres. The wave aberration can be decomposed through polynomials in a sum of pure aberration terms. The lower-degree terms correspond to the well-known optical aberrations: defocus and astigmatism.The following terms are the higher-order aberrations: coma, spherical aberration and trefoil. A convenient way of decomposing the wave aberration is to use the Zernike polynomial expansion[17]. Figure 1a shows schematically the two main optical components of the eye (cornea and lens) and an example of the wave aberration over the pupil and the retinal point-spread function. The eye is actually a non-centred optical system (see relevant axes in Fig. 1a), mainly because the fovea (the area on the retina with the highest density of photoreceptors and thus the best visual resolution) is decentred. The angle κ (also known as λ) is the angular distance between the line of sight and the pupillary axis.

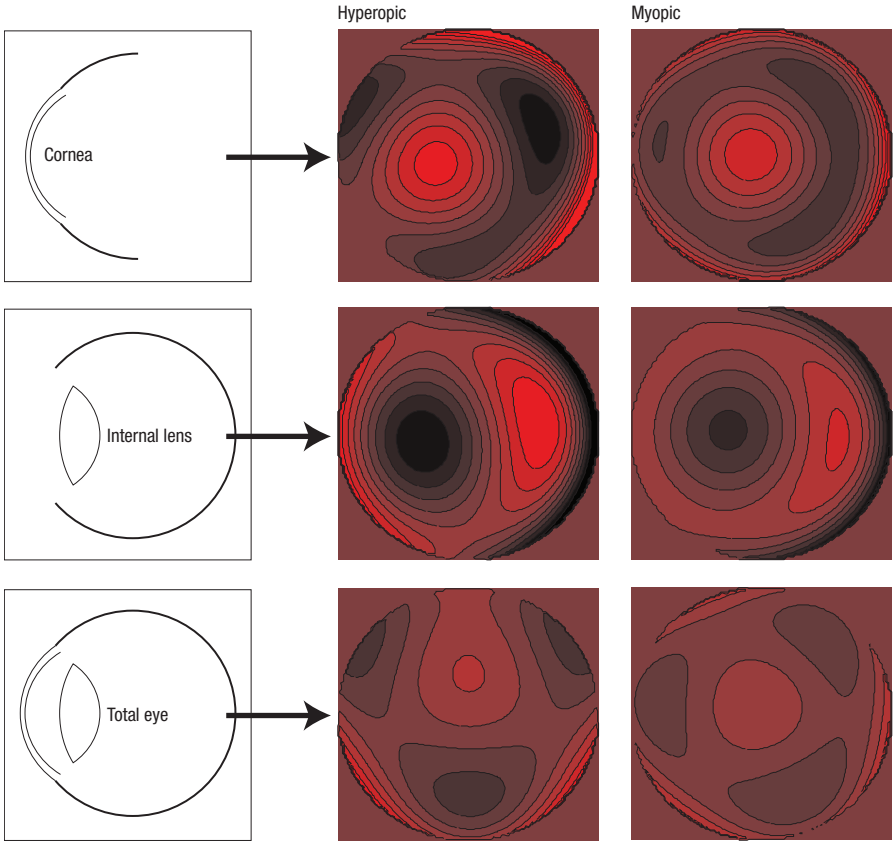

Figure 2 Average aberration maps for myopic and hyperopic groups, for each ocular component: cornea, internal lens and total eye. All data were obtained for a pupil of diameter 5 mm. The scale of the aberration maps is the same for all maps: from –0.5 μm to 0.5 μm.

The wave aberration of the complete eye can be measured using a variety of different subjective and objective techniques: 'vernier' alignment[18], the crossed cylinder aberroscope[19], calculations[20] from double-pass retinal images[21], and probably the most widely used method today, the Hartmann–Shack wavefront sensor[22,23]. The Hartmann–Shack wavefront sensor commonly consists of an array of microlenses, conjugated with the eye's pupil, and a camera placed at its focal plane. An infrared beam is projected onto the retina to produce a beacon image. Part of the light reflected in the retina leaves the eye and is captured by the sensor. If a perfect plane wavefront reaches the microlens array, the camera records a perfectly regular array of spots. However, if an aberrated wavefront reaches the sensor, the pattern of spots is irregular. The displacement of each spot from its ideal position is proportional to the derivative (gradient) of the wavefront over each microlens area. From the images of the spots, the ocular wave aberration is computed and expressed typically as a Zernike polynomial expansion.

The aberrations associated with the anterior surface of the cornea can be computed from its shape after measurement with corneal topography instruments. Once the cornea surface is determined, ray-tracing techniques through the corneal surface provide the associated aberrations[24].

It is also important to obtain the geometrical data of the eye's optical components. The location of the lens and the retina can be measured by using ultrasound techniques. In addition, recent optical techniques based on low-coherence interferometry[25] provide more accurate data. The anterior chamber of the eye can also be imaged by using both Scheimpflug photography[26] and optical coherence tomography[27]. In general, these techniques have a limited spatial resolution, and tomographic data cannot be used directly to compute the wave aberrations of each component. Another approach is to measure

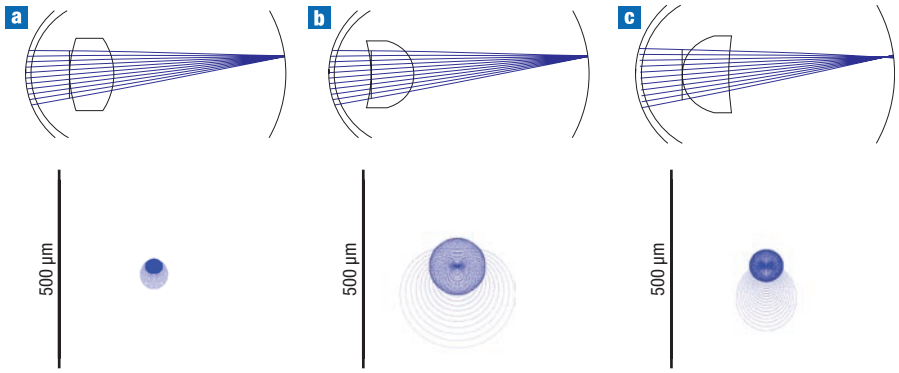

Figure 3 Three eye models with different shapes for the crystalline lens. **a**, The most realistic shape. **b**,**c**, Models that maintain the same optical power of the eye with non-physiological but optically possible shapes. The aberrations with the hypothetical shapes (**b**, **c**) are larger than with the realistic model. This can be observed from the interception plots of the rays with the retina shown below the models.

lens curvature, tilt and decentration by recording Purkinje images (images produced by reflection in the cornea and the lens). Different instruments based on this principle have been developed in recent years[28–30]. In addition to *in vivo* measurements, the crystalline lens has been extensively studied *in vitro* and information on the shape of surfaces and the distribution of the lens refractive index has been obtained[31].

MODELLING THE EYE'S OPTICS

Simple schematic models for the eye have been used for more than a century[32]. However, these types of simplified representation were developed with average data and had very limited potential for predicting the actual image properties of real eyes. Even when additional features were incorporated into the models[33], for instance aspheric surfaces or the gradient index of the lens, the performance of real eyes considerably differs from the predictions of schematic models.

A more powerful approach to understanding the eye's optics and to predicting with reasonable accuracy the aberration of a particular eye is the construction of individual (or customized) modelling. It is now possible to use experimental data (corneal shape, eye geometrical distances, surface alignments) to create individual, customized eye models. Predicted wavefront aberrations are then obtained by tracing finite rays for different model configurations using commercial ray-tracing software, such as ZEMAX or OSLO. The predictions of aberrations can then be compared with those measured in the same eye by the Hartmann–Shack wavefront sensor. Figure 1b shows a schematic representation of a personalized model.

ABERRATIONS IN NORMAL EYES

The magnitude of higher-order aberrations in normal subjects represents just a small fraction of the total aberrations of the eye. Lower-order aberrations — defocus and astigmatism — are responsible for most of the degradation in a retinal image. That said, it is still useful to understand and measure the effect of higher-order aberrations. Several research groups have studied the statistical distribution of higher-order aberrations[34,35]. In general, a large variability occurs between subjects. It is interesting that the structure of aberrations between left and right eyes has mirror symmetry, with most of the Zernike modes in one eye significantly correlated with their counterparts in the opposite eye.

The cornea represents two-thirds of the optical refractive power of the eye. It is the main refracting component of the eye and a major contributor to the total aberrations. Initial studies of corneal optics considered spherical aberration as its main higher-order aberration[36]. However, recent studies have shown how the magnitude of corneal coma can be as large as its spherical aberration[10]. This opened discussion about the role of the optical properties of the crystalline lens, because some of the aberrations in the cornea were not present in the total eye. This led to the conclusion that the optical aberrations of the lens must have, at some level, a compensatory effect on the corneal aberrations. It was also demonstrated that this compensation was larger in eyes with larger angles, typically hyperopic (far-sighted) eyes. Figure 2 shows examples of the average aberration maps for the cornea, lens and eye in a myopic (short-sighted) and hyperopic group of eyes. The compensation effects on spherical aberration and coma can be seen.

THE APLANATIC DESIGN OF THE EYE

An aplanatic optical system is a lens configuration forming images with minimal spherical aberration and off-axis coma. It is a well-known solution that is often used by optical designers. Using the lens shapes and other optical variables, it is possible to calculate all the aplanatic solutions for a two-lens optical system immersed in air[37]. These solutions are also of interest for the design of reflecting telescopes[38,39].

It is extraordinary to realize how the optical design of the human eye resembles the characteristics of one of these aplanatic optical systems, with the crystalline lens acting as an aspheric compensator for providing a (partial) correction of corneal spherical aberration and avoiding major generation of off-axis coma. Because the angle κ tends to be slightly larger for hyperopic eyes compared with myopic eyes, it is expected that a larger compensation effect exists for hyperopic subjects. It seems clear that this special design of the human eye is able to maintain constant optical quality independent of some alignment variables, thus making the design more robust and tolerant.

The choice of the lens shape, from an optical point of view, is clearly carefully optimized. Simulations comparing the eye's actual lens shape with other models of hypothetical crystalline lens shape (with the same optical power) show that, although they all achieve paraxial focus correctly on the retina, they are totally different in terms of the amount of coma. Figure 3 shows an eye model with a real crystalline lens shape and two other models with other hypothetical shapes. The graphs below the eye models show spot diagrams, with the more compact distribution (better image quality) obtained with the realistic model. As such, it is clear that the eye represents an elegant design that is optimized to minimize distortion and is capable of rendering a retinal image of high quality.

In conclusion, gaining a better understanding of the eye's optical properties will prove increasingly useful in the future and will certainly help to optimize approaches to vision testing and

correction. Ultimately it may be possible to develop a new generation of improved diagnostic, therapeutic and corrective instruments, based on advanced optical technologies that bring better visual care to the general population.

References

1. Liang, J., Williams, D. R. & Miller, D. T. *J. Opt. Soc. Am. A* **14,** 2884–2892 (1997).
2. Fernández, E. J., Iglesias, I. & Artal, P. *Opt. Lett.* **26,** 746–748 (2001).
3. Geary, J. M. *Introduction to Wavefront Sensors* (SPIE Press, Bellingham, USA, 1995).
4. Artal, P. & Guirao, A. *Opt. Lett.* **23,** 1713–1715 (1998).
5. Artal, P., Guirao, A., Berrio, E. & Williams, D. R. *J. Vis.* **1,** 1–8 (2001).
6. Kelly, J. E., Mihashi, T. & Howland, H. C. *J. Vis.* **4,** 262–271 (2004).
7. Artal, P., Benito, A. & Tabernero, J. *J. Vis.* **6,** 1–7 (2006).
8. Artal, P., Berrio, E., Guirao, A. & Piers, P. *J. Opt. Soc. Am. A* **19,** 137–143 (2002).
9. Glasser, A. & Campbell, M. C. W. *Vis. Res.* **38,** 209–229 (1998).
10. Guirao, A., Redondo, M. & Artal, P. *J. Opt. Soc. Am. A* **7,** 1697–1702 (2000).
11. Guirao, A. *et al. Arch. Ophthalmol.* **120,** 1143–1151 (2002).
12. Tabernero, J., Piers, P. & Artal, P. *Opt. Lett.* **32,** 406–408 (2007).
13. Tabernero, J., Piers, P., Benito, A., Redondo, M. & Artal, P. *Invest. Ophthalmol. Vis. Sci.* **47,** 4651–4658 (2006).
14. Rosales, P. & Marcos, S. *Opt. Express* **15,** 2204–2218 (2007).
15. Tabernero, J., Benito, A., Alcón, E., Artal, P. *J. Opt. Soc. Am. A* **24,** 3274–3283 (2007).
16. Smith, W. J. *Modern Optical Engineering* 3rd edn (McGraw Hill, New York, 2000).
17. Noll, R. J. *J. Opt. Soc. Am.* **66,** 207–211 (1976).
18. Smirnov, M. S. *Biofizika* **6,** 776–795 (1961).
19. Howland, H. C. & Howland, B. *J. Opt. Soc. Am.* **67,** 1508–1518 (1977).
20. Iglesias, I., Berrio, E. & Artal, P. *J. Opt. Soc. Am. A* **15,** 2466–2476 (1998).
21. Santamaría, J., Artal, P. & Bescós, J. *J. Opt. Soc. Am. A* **4,** 1109–1114 (1987).
22. Liang, J., Grimm, B., Goelz, S. & Bille, J. F. *J. Opt. Soc. Am. A* **11,** 1949–1957 (1994).
23. Prieto, P. M., Vargas-Martín, F., Goelz, S. & Artal, P. *J. Opt. Soc. Am. A* **17,** 1388–1398 (2000).
24. Guirao, A. & Artal, P. *J. Opt. Soc. Am. A* **17,** 955–965 (2000).
25. Fercher, A., Mengedoht, K. & Werner, W. *Opt. Lett.* **13,** 186–188 (1988).
26. Cook, C. & Koretz, J. *J. Opt. Soc. Am. A* **15,** 1473–1485 (1998).
27. Fercher, A., Drexler, W., Hitzenberger, C. K. & Lasser, T. *Rep. Prog. Phys.* **66,** 239–303 (2003).
28. Barry, J. C., Dunne, M. C. M. & Kirschkamp, T. *Ophthalmic. Physiol. Opt.* **21,** 450–460 (2001).
29. Rosales, P. & Marcos, S. *J. Opt. Soc. Am. A* **23,** 509–520 (2006).
30. Tabernero, J., Benito, A., Nourrit, V. & Artal, P. *Opt. Express* **14,** 10945–10956 (2006).
31. Glasser, A. & Campbell, M. C. W. *Vision Res.* **39,** 1991–2015 (1999).
32. Gullstrand, A. in *Handbuch der Physiologischen Optik* 3rd edn, 1909 Vol. 1 (ed. Southall, J. P.) 351–352 (Optical Society of America, Washington DC, 1924).
33. Liou, H. L. & Brennan, N. A. *J. Opt. Soc. Am. A* **14,** 1684–1695 (1997).
34. Porter, J., Guirao, A., Cox, I. G. & Williams, D. R. *J. Opt. Soc. Am. A* **18,** 1793–1803 (2001).
35. Thibos, L. N., Hong, X., Bradley, A. & Cheng, X. *J. Opt. Soc. Am. A* **19,** 2329–2348. (2002).
36. Kiely, P. M., Smith, G. & Carney, L. G. *Opt. Acta* **29,** 1027–1040 (1982).
37. Jamieson, T. H. *Appl. Opt.* **15,** 2276–2282 (1976).
38. Head, A. K. *Proc. Phys. Soc. B*, **70,** 945–949 (1957).
39. Hannan, P. G. *Appl. Opt.* **31,** 513–518 (1992).

Acknowledgements

Our work is supported in part by the Ministerio de Educación y Ciencia, Spain (grants FIS2004-2153 and FIS2007-64765) and Fundación Séneca, Murcia, Spain (04524/GERM/06). We thank the members of our laboratory for their contributions to some specific parts of the reviewed research.